Precision Engineering 73 (2022) 203–213

Contents lists available at ScienceDirect

Precision Engineering

journal homepage: www.elsevier.com/locate/precision

Depolarization of surface scattering in polarized laser scattering detection for machined silicon wafers

Jingfei Yin [a], Qian Bai [b], Han Haitjema [c], Bi Zhang [d,*]

[a] College of Mechanical and Electrical Engineering, Nanjing University of Aeronautics and Astronautics, Nanjing, 210016, China
[b] School of Mechanical Engineering, Dalian University of Technology, Dalian, 116024, China
[c] Department of Mechanical Engineering, KU Leuven, Leuven, 3001, Belgium
[d] Department of Mechanical and Energy Engineering, Southern University of Science and Technology, Shenzhen, 518055, China

ARTICLE INFO

Keywords:
Polarized laser scattering
Depolarization
Surface roughness
Subsurface damage
Monocrystalline silicon

ABSTRACT

Monocrystalline silicon is currently one of the most used materials in the semiconductor industry. However, being hard and brittle, a silicon wafer commonly suffers from machining-induced subsurface damage (SSD). Detecting SSD is important for optimizing the machining process in order to improve the surface integrity of a machined wafer. Among the various detection methods, the polarized laser scattering (PLS) method has a huge potential in highly efficient detection. However, the surface scattering mechanism is not fully understood so far, which impedes the optimization of the PLS detection processes. This study resolves surface scattering based on the electromagnetic scattering theory. It is found that the depolarization caused by surface scattering increases with the surface roughness and the incident angle. With the consideration of the subsurface scattering characteristics and the distribution of the SSD, this study provides a solution for the PLS detection that comprises of the use of a horizontally polarized laser with vertical incidence to minimize the influence of surface scattering. This study provides a theoretical analysis of both surface and subsurface scattering to facilitate an optimized PLS detection.

1. Introduction

Monocrystalline silicon is widely used in semiconductor, new energy [1], optical [2], sensor [3], and detection industries [4] because of its excellent physical, mechanical, and electronic properties. It still represents a huge prospect of application in the foreseeable future. In order to meet the requirements regarding geometrical shape and size of a part, the monocrystalline silicon is subject to various machining processes. Since monocrystalline silicon is hard and brittle, it is inevitable to induce subsurface damage (SSD) into a machined surface. Subsurface damage degrades the surface integrity and may lead to warpage and cracking, which is detrimental to the service life and performance of a silicon chip. Therefore, it is necessary to suppress and remove SSD.

Detecting SSD can provide a comprehensive evaluation for a machining process, which is important for optimizing the machining parameters and the SSD removal processes. However, since SSD is usually distributed underneath a machined surface, it is rather difficult to detect SSD in a machined silicon wafer. Generally, there are two kinds of methods for SSD detection, namely destructive and non-destructive methods, as reviewed by Yin et al. [5]. Although destructive methods are widely adopted to characterize SSD because of its reliability and accuracy, almost all the destructive methods suffer from limitations associated with low efficiency, high cost, and localized area of detection, in addition to the destruction of the sample to be analyzed. Non-destructive methods not only provide high detection efficiency with global information on SSD, but also they preserve the sample, which is highly attractive for application in practical production processes.

In order to rapidly obtain the SSD distribution information in a machined silicon wafer, many analytical models were proposed. Li et al. [6] established a predictive model for the SSD depth based on the surface roughness parameter *Rz* of a ground silicon wafer. The effects of the ductile machining, temperature, and crystal orientation were taken into consideration. However, the detection accuracy was compromised when the surface roughness parameter *Rz* of a sample being analyzed was smaller than 1 μm. Zhang et al. [7] proposed an analytical model to predict the SSD depth in self-rotation grinding of silicon wafers with the considerations of elastic recovery, cleavage plane, and crystallographic

* Corresponding author.
E-mail address: zhangb@sustech.edu.cn (B. Zhang).

https://doi.org/10.1016/j.precisioneng.2021.09.011
Received 24 March 2021; Received in revised form 3 September 2021; Accepted 13 September 2021
Available online 16 September 2021

orientation of the workpiece. Nonetheless, most works used the median crack depth to represent the SSD depth in the models, which inevitably results in erroneous predictions. This is due to the fact that the monocrystalline silicon is anisotropic. Machining-induced cracks tend to form in preferred cracking directions, i.e., cleavage planes, which makes the median crack oblique to the machined surface [8]. Therefore, the depth of a median crack is generally smaller than the extending length, which can cause prediction errors of up to 60%. Wang et al. [9] stated that it was more reasonable to use the maximum extending length of the half-penny crack system instead of the median crack depth. The analytical models can demonstrate the evolution of SSD in variable machining parameters. However, none of the models could precisely predict the SSD depth and distributions within a machined workpiece, due to the fact that SSD prediction can easily be influenced by many factors, such as machining process parameters, abrasive geometries, coolant application, and tool wear.

Popovich et al. [10] used computer tomography (XCT) to detect the internal microstructure of silicon solar cells. 3D images were generated with a maximum resolution of less than 0.5 μm. However, it took 90 min to scan a sample of 10 mm × 10 mm. Besides the low detection efficiency, the sample size was greatly limited, which impedes its practical applications.

Brand et al. [11] used scanning acoustic microscopy in the GHz range to detect the debonded defects within a silicon sample used for microelectronics. The shear wave and mixed mode were used to enhance the sensitivity for defect detection. The use of GHz-acoustic microscopy increased the spatial resolution, however, they could not simultaneously achieve both high accuracy and large detection area. Increasing the acoustic frequency increased the spatial resolution but decreased the acoustic penetration, which reduced the detection depth. Karabutov and Podymova [12] applied the laser-ultrasonic method for detecting the machining-induced SSD in the monocrystalline silicon, and reported that the minimal detectable depth of SSD was in the range of 0.15–0.2 μm after the received signal was mathematically processed with their specially designed algorithms and computer codes. However, the specially designed algorithms and computer codes were not provided.

Considering the ultrasonic propagation characteristics, the received ultrasonic signal is easily interfered by the surface waves dominated by workpiece surface roughness and the noise from the acoustic parts during the ultrasonic propagation. Shekhawat et al. [13] developed a scanning near-field thickness resonance acoustic microscope (SNTRAM) which combined the ultrasonic detection with an atomic force microscope platform. This SNTRAM was demonstrated to be able to detect subsurface defects with a high signal-to-noise ratio and high resolution. It could provide a lateral resolution of 5–8 nm in detecting an artificial subsurface structure. However, the surface of the sample used for detecting this was extremely smooth. In practice, a machined silicon surface is generally rough. The surface roughness certainly affects the ultrasonic propagation, which makes the selection of the useful signal tricky [13]. The influence of the surface roughness of a machined silicon wafer on detection resolution impedes the application of SNTRAM.

The influence of surface roughness could be minimized by using the polarization of light. Geiler et al. [14] proposed the scanning infrared depolarization (SIRD) method for achieving a rapid detection of the defects in silicon. The SIRD method took 3 min to achieve a full measurement of a 300-mm diameter silicon wafer, which was highly efficient. Geiler et al. [15] used SIRD to distinguish the SSD distribution of a silicon wafer subjected to different machining processes, however without any information on the depth resolution of SSD. Their results showed that the SIRD method was sensitive to the SSD distribution, simply because it was based on the photoelasticity principle.

Zhang et al. [16] worked on a polarized laser scattering (PLS) method, the cross-polarization confocal microscopy (CPCM), to detect SSD in silicon wafers. They found that surface scattering had little influence on detection. The encouraging results were obtained with CPCM. SSD was represented by bright speckles in the scanning images. SSD at different depth could be detected by a laser with different wavelengths. However, no quantitative correlation between scattering images and SSD depth was obtained. Zhang and Sun [17] indicated that by using different wavelength lasers, a correlation could be established between the laser scattering data and SSD depth.

Besides SSD, stress-induced photoelasticity also affects the PLS detection. Yin et al. [18] elaborated the depolarization mechanisms of the stress-induced photoelasticity and SSD scattering. They suggested that the photoelasticity could be minimized by aligning the polarization direction to a principal stress direction. They further revealed that both the SSD depth and distribution density in a ground silicon wafer affects the polarized laser scattering detection, with SSD depth being the dominant factor [19]. PLS provides a potential for detecting SSD in monocrystalline silicon. Unfortunately, surface scattering in PLS has generally been neglected and an analytical solution of the influence from the surface scattering is still absent.

Although the influence of surface roughness was experimentally demonstrated to be a minor factor to the PLS detection, the unrecovered surface scattering impedes the optimization of the PLS system design and drags the progress in the PLS detection. In order to recover the surface scattering in PLS detection, it is necessary to establish a theoretical scattering model. Zhang [20] analyzed the depolarization of the CPCM detection based on the Rayleigh scattering theory which, however, generally handles the scattering by a spherical scatter [21] instead of a rough surface. In addition to the light scattering theory, the electromagnetic (EM) scattering theory could be an alternative to deal with the surface scattering as a laser beam is also an EM wave.

The EM scattering theory is widely applied to the areas of radar detection and remote sensing. Two methods, i.e., numerical and analytical, are available to resolve the EM scattering of a rough surface. The numerical method, e.g., the method of moments (MOM) [22], finite element method (FEM) [23], and finite difference time domain (FDTD) [24], can precisely resolve the surface EM scattering of a part in a complex geometrical shape. However, such a method requires a large amount of computation for an accurate result, which limits its practical application.

On the other hand, the analytical method is more convenient to use because of the compromise between the computation accuracy and efficiency. The application of the analytical method is dependent on surface roughness [25]. For a surface with roughness much smaller than the wavelength of the incident EM wave, the small perturbation method (SPM) is applicable. However, the dimensions associated with the roughness of a machined silicon wafer are generally larger than the incident laser wavelength. For the surfaces with much larger roughness dimensions compared to the laser wavelength, the geometrical optics (GO) approximation is widely applied. However, in the case of sharp incident angles, GO is based on the specular reflection without taking the multi-scattering into consideration, which leads to a calculated scattering that is independent of the polarization of the incident beam. For the surfaces with intermediate roughness scales, there are many methods available, such as the two-scale model (TSM), and the small slope approximation (SSA) [26]. However, the surfaces with intermediate roughness scales generally refer to natural interfaces or sea surface [25], rather than the machined silicon surface.

Generally, if single scattering takes place at the surface, the polarization preserves, otherwise, the scattering light is depolarized if the incident light is multi-scattered. Fung et al. [27] proposed a model by integrating the single scattering and multi-scattering. In this way, the scattering for both small and large surface roughness parameters are all considered, which provides a chance to resolve the surface scattering of a machined silicon in the PLS detection.

Given the unclear surface scattering of a machined silicon wafer in the PLS detection, this study is to establish a scattering model to clarify the surface scattering characteristics. Based on the model, both the surface scattering and subsurface scattering in the PLS detection of a machined silicon wafer are to be resolved. Then, the influence of surface

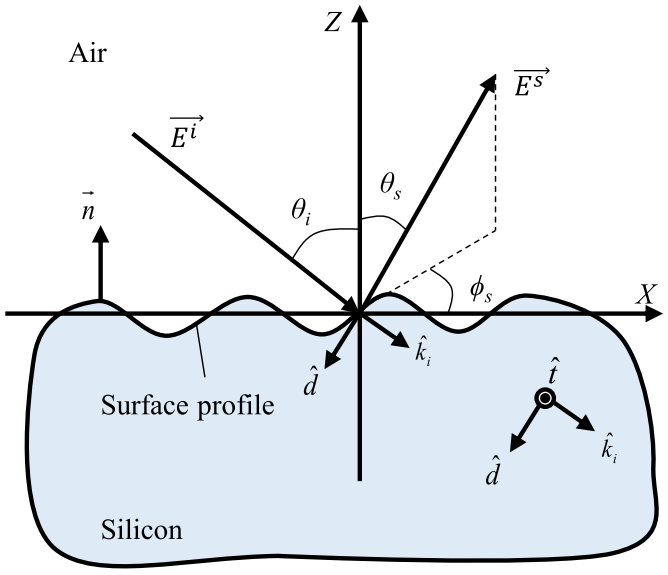

Fig. 1. Schematic diagram of surface scattering.

roughness to the PLS detection is determined. Thereby, the PLS detection mechanism and characteristics can be elaborated. According to the distribution of SSD in the machined silicon wafer, this study is to propose a system design for the PLS detection to minimize the surface roughness influence and detect the SSD in the machined silicon wafer, as well as install the designed PLS detection system. Finally, the influence of surface roughness and SSD in the detection using the installed PLS detection system is to be experimentally verified. Therefore, the scattering model of the PLS detection can be rationalized and the feasibility of the installed PLS detection system can be demonstrated. Therefore, this study theoretically resolves the PLS scattering and provides a guide for the system design of the PLS detection, which is significant for optimizing the PLS detection of machining-induced SSD in monocrystalline silicon.

2. Polarized laser scattering modelling

When a wavefront emerging from a laser light source encounters a silicon surface, the light is scattered by the surface asperities, as shown in Fig. 1. $\vec{n}$ is the normal vector of the silicon surface. $\hat{t}$, $\hat{d}$, are the unit vectors of the local coordinates. $\hat{x}$, $\hat{y}$, and$\hat{z}$ are the unit vectors of the global coordinates. θ_i, θ_s, and φ_s are the incident angle, the scattering angle, and the azimuth angle of the scattering light, respectively. The EM field of the incident polarized laser beam can be expressed as Eq. (1).

$$\begin{cases} \vec{E}^i = \hat{p}E_i e^{-j\vec{k}\cdot\vec{r}} = \hat{p}E^i \\ \vec{H}^i = \hat{k}_i \times (\hat{p}E^i) \end{cases} \tag{1}$$

where $\hat{p}$ is the unit polarization vector of the incident beam; E_i is the amplitude of the electric field; $\vec{k}_i = k\cdot\hat{k}_i$, k is the wave number of the incident beam,$k = 2\pi/\lambda$; $\hat{k}_i$ is the unit$\hat{k}_i$ vector in the incident direction; and λ is the wavelength of the incident beam. The far-zone surface scattering EM field can be written as Eq. (2), as indicated by Fung et al. [27].

$$E^s_{pq} = C\int\left[\vec{k}_i \times \vec{q}\cdot\left(\vec{n}\times\vec{E}^i_p\right) + \vec{q}\cdot\left(\vec{n}\times\vec{H}^i_p\right)\right]\cdot\exp\left(-j\vec{k}_i\vec{r}\right)ds \tag{2}$$

where $\vec{k}_i = k(\hat{x}\sin\theta_i - \hat{z}\cos\theta_i) = \hat{x}k_x - \hat{z}k_z$; $C = -\frac{jk}{4\pi R}\exp(-jkR)$; $\vec{q}$ is the unit polarization vector of the received scattering light; R represents the distance from the scattering point. The polarization of the incident light is p while the polarization of the scattering light is q. The unit vectors of the polarization are shown as Eq. (3).

$$\begin{cases} \hat{h} = \hat{y} \\ \hat{v} = \hat{x}\cos\theta_i + \hat{z}\sin\theta_i \end{cases} \tag{3}$$

where $\hat{h}$ represents the horizontal polarization, i.e., s-polarization whose polarization direction is perpendicular to the incident plane, $\hat{v}$ represents the vertical polarization whose polarization direction is parallel to the incident plane, i.e., p-polarization.

However, Eq. (2) does not directly resolve the surface dependent scattering. Li and Fung [28] stated that the scattering EM could be written as a sum of the standard Kirchhoff surface field and a complementary surface field, as shown in Eq. (4).

$$E^s_{pq} = E^k_{pq} + E^c_{pq} \tag{4}$$

The standard Kirchhoff surface field and the complementary surface field are resolved by Fung et al. [27], given by Eqs. (5) and (6), respectively.

$$E^k_{pq} = CE_i\int f_{pq}\exp\left(-2j\vec{k}_i\cdot\vec{r}\right)dxdy \tag{5}$$

$$E^c_{pq} = \frac{CE_i}{8\pi^2}\int F_{pq}\exp\left[ju(x-x') + jv(y-y') - j\vec{k}_i\cdot\vec{r} - j\vec{k}_i\cdot r'\right]dxdydx'dy'dudv \tag{6}$$

where f_{pq} and F_{pq} are generally the rough surface spatial variable-dependent dimensionless constants. Considering the linear polarization of the incident EM wave, Fung et al. [27] ingeniously derived the explicit approximate expressions of the two dimensionless constants which are independent of the spatial variables but highly dependent on the reflection coefficient of the surface. Therefore, the power of the backscattered light can be determined by

$$P_{pq} = \langle E^s_{pq}E^{s\,*}_{pq}\rangle = \langle E^k_{pq}E^{k\,*}_{pq}\rangle + 2\mathrm{Re}\langle E^c_{pq}E^{k\,*}_{pq}\rangle + \langle E^c_{pq}E^{c\,*}_{pq}\rangle \tag{7}$$

Then, a backscattering coefficient is given by Eq. (8).

$$C_{pq} = \left(4\pi R^2 P_{pq}\right) / \left(E_i^2 A_i\right) \tag{8}$$

where A_i is the radiation area of the incident beam. Finally, the backscattering coefficient is resolved into two terms, namely the single scattering coefficient $C^{(S)}_{pq}$ and the multi-scattering coefficient$C^{(M)}_{pq}$, as shown in Eq. (9).

$$C_{pq} = C^{(S)}_{pq} + C^{(M)}_{pq}. \tag{9}$$

Since the single scattering does not change the polarization of the scattering light, the depolarization of surface scattering is mainly dependent on the multi-scattering. Fung et al. [27] summarized two expressions of the multi-scattering coefficient for two kinds of surface, $k\sigma < 3$ and $k\sigma > 3$. σ is the standard deviation of the surface profile from a flat, representing surface roughness. For monocrystalline silicon, grinding is the mostly used machining process, which makes the standard deviation σ of a ground surface small enough to satisfy $k\sigma < 3$. Therefore, the multi-scattering coefficient in Eq. (9) is given as Eq. (10).

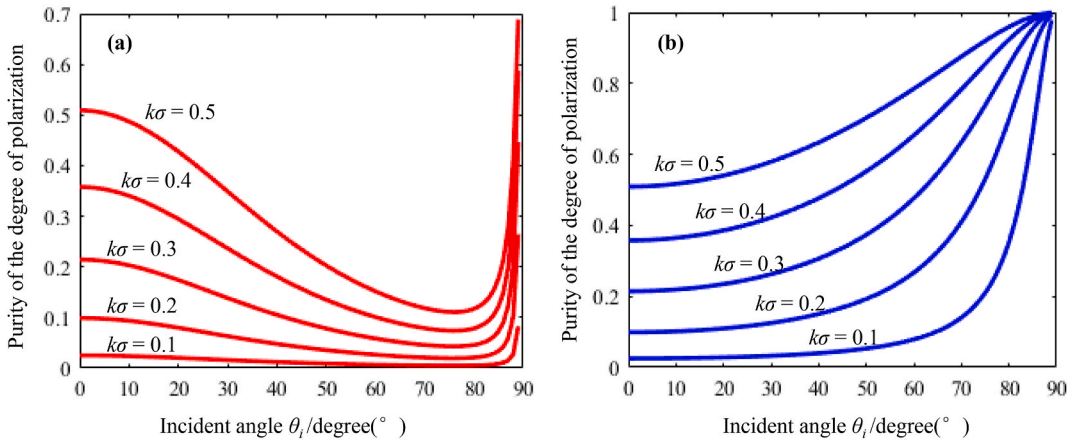

Fig. 2. The influences of the surface roughness to the purity of the degree of polarization D for the incident laser beam with (a) p-polarization and (b) s-polarization. (laser wavelength $\lambda = 914$ nm and surface parameter $kS_{al} = 1$).

$$C_{pq}^{(M)} = \frac{k^2}{4\pi}\exp\left(-3k_z^2\sigma^2\right)\sum_{n=1}^{\infty}\sum_{m=1}^{\infty}\frac{\left(2k_z^2\sigma^2\right)^{n+m}}{n!m!}\cdot\int \mathrm{Re}\left[f_{pq}^{*}F_{pq}(u,v)\right]W^n(u-k_x,v)\cdot W^m(k_x+u,v)dudv$$
$$+\frac{k^2}{16\pi}\exp\left(-2k_z^2\sigma^2\right)\sum_{n=1}^{\infty}\sum_{m=1}^{\infty}\frac{\left(k_z^2\sigma^2\right)^{n+m}}{n!m!}\cdot\int\left[\left|F_{pq}(u,v)\right|^2+F_{pq}^{*}(u,v)F_{pq}^{*}(-u,-v)\right] \tag{10}$$
$$\cdot W^m(u-k_x,v)\cdot W^n(u+k_x+u,v)dudv$$

where k_z is the wave number along the Z axis, $k_z = k\cdot\cos\theta_i$, f_{pq}^{*} and F_{pq}^{*} are the complex conjugates of f_{pq} and F_{pq}, and σ^2 and W are the variation and power spectral density function of the silicon surface, respectively.

By expanding the series and substituting the explicit expressions of the dimensionless constants, the multi-scattering coefficients are derived, as shown in Eq. (11).

$$\begin{cases} C_{pp} = 8k^4\sigma^2\left|r_p\cos^2\theta_i + \dfrac{\sin^2\theta_i\left(1+r_p\right)^2}{2}\left(1-\dfrac{1}{\varepsilon_r}\right)\right|^2\cdot W(-2k_x,0) \\ C_{ss} = 8k^4\sigma^2\left|r_s\cos^2\theta_i\right|^2\cdot W(-2k_x,0) \\ C_{sp} = C_{ps} = \dfrac{8k^4\sigma^4\cos^2\theta_i}{\pi}\exp\left(-2k_z^2\sigma^2\right)\displaystyle\int\int\frac{u^2v^2}{q^2}W(u-k_x,v)\cdot\ W(u+k_x,v)dudv \end{cases} \tag{11}$$

where$q = \sqrt{k^2-u^2-v^2}$,ε_r is the dielectric coefficient and permeability of monocrystalline silicon, r_p and r_s are the amplitude reflection coefficient of the p-polarization and s-polarization lights, respectively. The amplitude reflection coefficient refers to the ratio of the amplitude of scattering light to that of the incident light, it is not the intensity ratio of the scattering light to incident light which was well illustrated in the work by Haitjema [29].The expressions of the amplitude reflection coefficient, also known as the Fresnel coefficients, are shown in Eq. (12).

$$\begin{cases} r_p = \dfrac{n^2\cos\theta_i - \sqrt{n^2-\sin^2\theta_i}}{n^2\cos\theta_i + \sqrt{n^2-\sin^2\theta_i}} \\ r_s = \dfrac{\cos\theta_i - \sqrt{n^2-\sin^2\theta_i}}{\cos\theta_i + \sqrt{n^2-\sin^2\theta_i}} \end{cases} \tag{12}$$

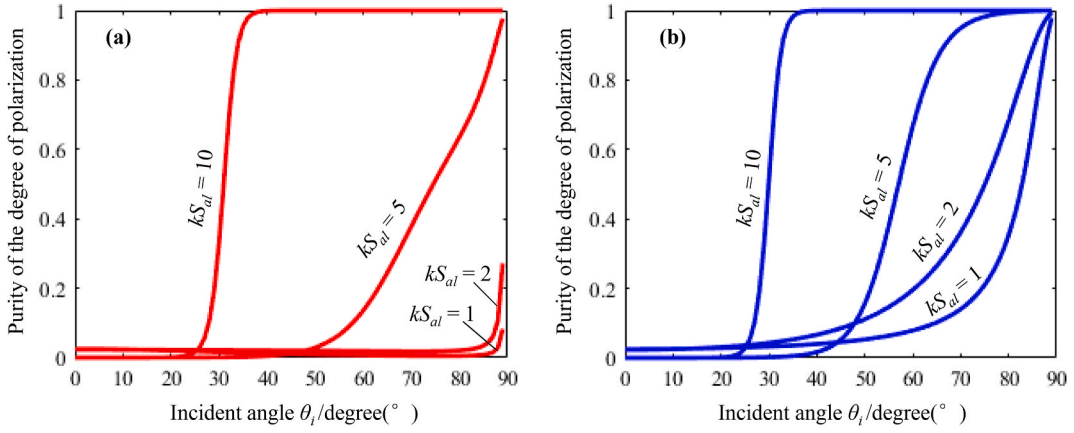

Fig. 3. The influence of the surface correlation length to the purity of the degree of polarization D for the incident laser beam with (a) p-polarization and (b) s-polarization.

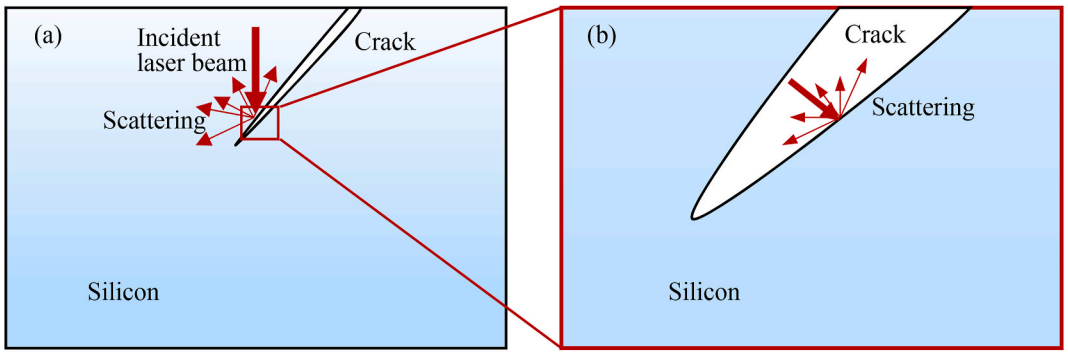

Fig. 4. Schematics of subsurface scattering at (a) silicon-to-crack interface and (b) crack-to-silicon interface. (For interpretation of the references to colour in this figure legend, the reader is referred to the Web version of this article.)

where n is the refractive index of the monocrystalline silicon. Then, by expanding the surface power spectral density function, the ultimate expressions of the multi-scattering coefficients, namely preserved-polarization scattering coefficients C_{ss} and C_{pp} and cross-polarization scattering coefficients C_{sp} and C_{ps}, are shown in Eq. (13).

$$\begin{cases} C_{pp} = 4k^4 S_{al}^2 \sigma^2 \cdot \exp\left(-k^2 S_{al}^2 \sin^2\theta_i\right) \cdot \left| r_p \cos^2\theta_i + \dfrac{\sin^2\theta_i \left(1+r_p\right)^2}{2}\left(1-\dfrac{1}{\varepsilon_r}\right)\right|^2 \\ C_{ss} = 4k^4 S_{al}^2 \sigma^2 \cdot \exp\left(-k^2 S_{al}^2 \sin^2\theta_i\right) \cdot \left| r_s \cos^2\theta_i \right|^2 \\ C_{sp} = C_{ps} = \dfrac{2k^4 S_{al}^2 \sigma^4 \cos^2\theta_i}{\pi} \exp\left(-\dfrac{k^2 S_{al}^2 \sin^2\theta_i}{2}\right) \exp\left(-2k^2\sigma^2\cos^2\theta_i\right) \int\int \dfrac{u^2 v^2}{k^2-u^2-v^2} \exp\left[-\dfrac{S_{al}^2\left(u^2+v^2\right)}{2}\right] dudv \end{cases} \tag{13}$$

where S_{al} is the correlation length of the silicon surface. It can be found that the multi-scattering coefficients are dependent on surface roughness, laser incident angle, surface profile, and polarization of the incident beam. Therefore, it is necessary to study the influence of surface scattering in the PLS detection.

3. Polarized laser scattering analysis

In the PLS detection, the main concern is the depolarization which takes places after scattering. In this study, the purity of the degree of polarization is defined as the ratio of the cross-polarization scattering coefficient to the sum of the cross-polarization scattering coefficient and the preserved-polarization scattering coefficient, as shown in Eq. (14).

$$D = \frac{C_{pq}}{C_{pq} + C_{pp}} \tag{14}$$

Therefore, $D = 0$ means the scattering light is not depolarized. $D = 1$ means the scattering light is fully depolarized. Based on Eqs. (13) and (14), the PLS characteristics are studied as follows.

3.1. Surface scattering

Since the incident laser beam wavelength can be variable, ranging from extreme ultraviolet to far infrared, in surface scattering the surface parameters are compared with the wavelength of the incident beam. Generally, the products of the wave number of the incident laser beam with the surface parameters are used to indicate the surface roughness in PLS. The influences of the surface roughness to the scattering

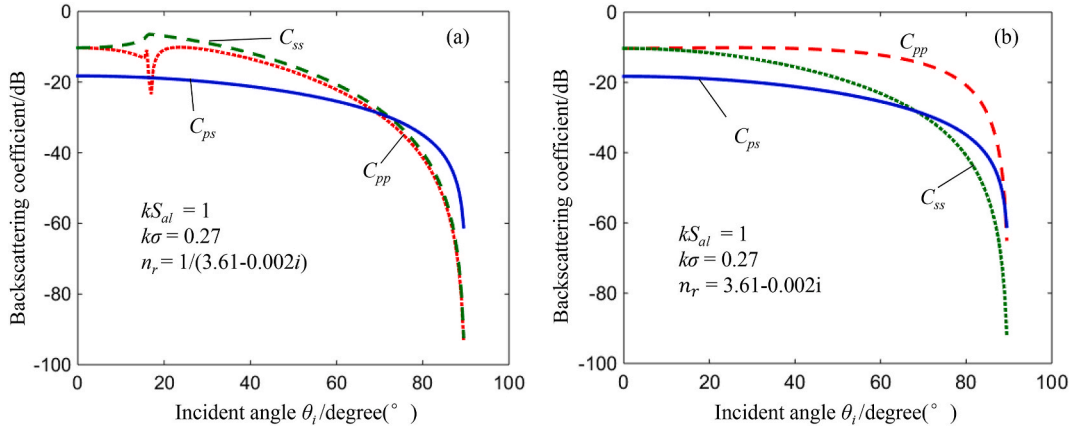

Fig. 5. The variation of the backscattering coefficient with incident angle in scattering at (a) silicon-to-crack interface and (b) crack-to-silicon interface. (For interpretation of the references to colour in this figure legend, the reader is referred to the Web version of this article.)

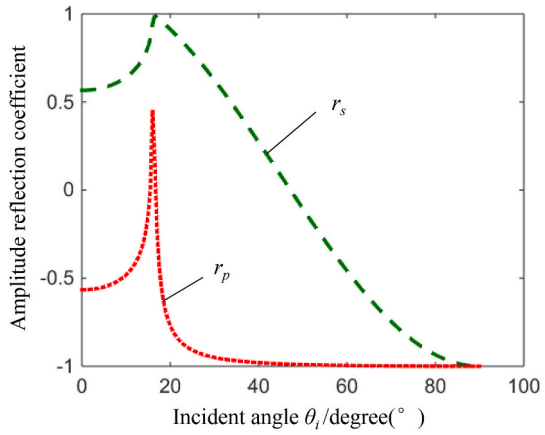

Fig. 6. The real part of the amplitude reflection coefficients as a function of the incident angle of the polarized light, calculated from Eq. (12).

depolarization as calculated from Eqs. (13) and (14) are shown in Fig. 2. Generally, the purity of the degree of polarization D increases with the surface roughness due to large surface asperities which causes multi-scattering. For different polarizations of the incident beam, i.e., p- and s-polarizations, the depolarization variations with the incident angle are quite different. For the incident beam with the p-polarization, as shown in Fig. 2(a), the purity of the degree of polarization of the scattering light decreases with an increase in the incident angle from zero to about 80° after which D dramatically increases. For the incident beam with s-polarization, as shown in Fig. 2(a), D monotonically increases with the incident angle. Therefore, it is important for the PLS detection to take the polarization of incident beam into consideration.

In addition to the surface roughness, the surface correlation length is another important parameter for the PLS detection. The influence of the surface correlation length to the surface scattering depolarization is shown in Fig. 3. Generally, the purity of the degree of polarization D increases with the surface correlation length. On the other hand, the variation of the purity of the degree of polarization with the incident angle is unitary. The purity of the degree of polarization increases with the incident angle for both the p-polarization and s-polarization cases. It is found that D is stable at a low value close to zero when the incident angle is small enough. At an increased incident angle, D dramatically increases to one, i.e., the beam is fully depolarized. Therefore, based on the surface scattering characteristics, it is reasonable for the PLS detection to make the incident angle of the laser small enough, i.e., vertical incidence to the silicon surface, to minimize the surface scattering influence.

It has to be mentioned here that the machined surface slope (*Rdq*) is assumed to be large. As stated by Fung et al. [27], if the surface roughness was large but the surface slope is small, only the single scattering was significant, which would preserve the polarization of the scattering light. If the surface slope was large, the multi-scattering would also be significant. Multi-scattering would correspondingly lead to the depolarization of the scattering light. Besides, the small surface slope generally exists on the natural terrains. Therefore, for a machined surface of monocrystalline silicon, the surface slope should be large, so that the surface scattering including the multi-scattering has to be taken into consideration in the PLS detection.

3.2. Subsurface scattering

Because the PLS method is applied to detect SSD, it is necessary to take the subsurface scattering into consideration. As already stated, the EM scattering theory is also applicable to describing the subsurface scattering. Due to the discontinuity caused by SSD, the subsurface scattering is classified into two cases, as shown in Fig. 4: (a) the scatterings at silicon-to-crack (STC) interface and (b) crack-to silicon (CTS) interface.

The refractive index of silicon is different from that of air, which results in the difference in the scattering characteristics at STC and CTS interfaces. Based on Eqs. 12–14, the backscattering coefficient at different incident angles are calculated. The variations of the backscattering coefficients with the incident angle in the two cases are shown in Fig. 5. It is notable that in the two cases, the backscattering coefficient decreases with increasing incident angle. Especially, when the incident angle is larger than 80°, the backscattering coefficient dramatically decreases to below −40 dB which is far less than that in the scattering at smaller incident angles. Therefore, scattering at the grazing incidence could be neglected. As shown in Fig. 5 (a), at the incident angle of about 18°, the preserved-polarization backscattering coefficients present pop-in peaks which are caused by the total reflection at the STC interface. Since the refractive index of silicon is larger than air, the total reflection occurs when the light passes through the STC interface. As shown in Fig. 6, the reflection of the polarized light is highly dependent on the incident angle. At the incident angle close to 18°, the reflection of the p-polarization light decreases to zero and then goes up and down with 180° phase difference. Meanwhile, the amplitude reflection coefficient of the s-polarization light increases to one.

The depolarization characteristics of the scatterings in the two cases are shown in Fig. 7. At the STC interface, there is a favorable incident angle range, just over the total reflection angle, within which depolarization is much more significant using the incident laser beam with p-polarization compared to s-polarization, which is beneficial for detecting SSD. Otherwise, the depolarization of the scattering is similar, as

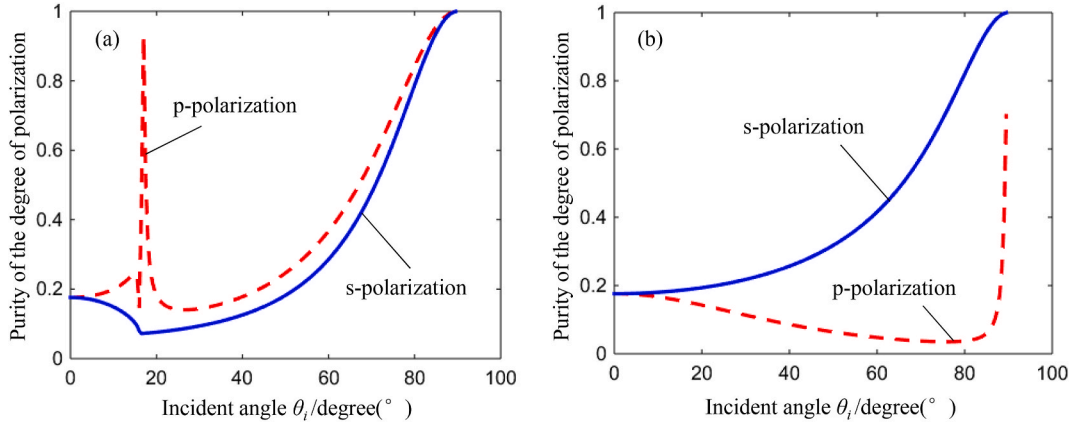

Fig. 7. The depolarization characteristics of scatterings at (a) silicon-to-crack interface and (b) crack-to-silicon interface. (For interpretation of the references to colour in this figure legend, the reader is referred to the Web version of this article.)

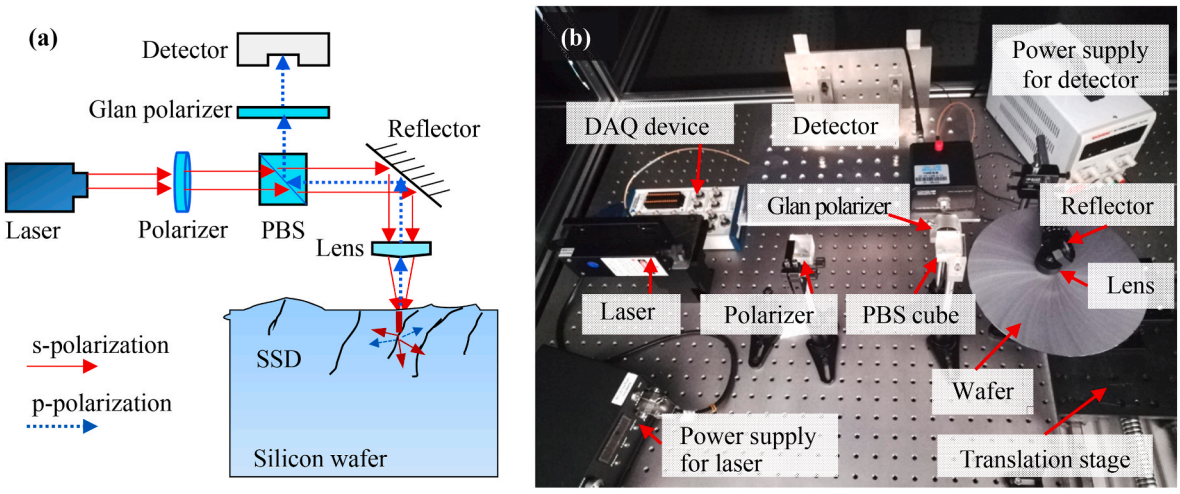

Fig. 8. PLS detection system (a) schematic diagram of the laser path, (b) photographical view.

shown in Fig. 7 (a). The significant increase in the depolarization of p-polarization is due to the change in backscattering coefficient. By comparing Figs. 5(a), 6 and 7(a), it is easy to find that the favorable incident angle range is close to the total reflection angle. Near the total reflection angle, as shown in Fig. 5(a), when incident laser is p-polarized, the polarization reservation backscattering coefficient C_{pp} first dramatically decreases to below the polarization alternation backscattering coefficient C_{ps} and then increases over C_{ps}. Correspondingly, based on Eq. (14), the depolarization in the case of the p-polarized light incidence represents a significant peak in the favorable incident angle range. The scattering at the CTS interface is different. As shown in Fig. 7 (b), s-polarization incidence leads to obviously more depolarization than p-polarization incidence in the full range of incident angles.

Although Fig. 5 (a) shows that using the p-polarized incident beam presents a huge advantage over the s-polarized in the advantageous angle range at the STC interface, the advantageous angle range is rather narrow, which puts a high requirement on the alignment of the PLS detection. However, SSD in the machined silicon is in complex shapes, as revealed by Pei et al. [30]. The inclination angle of SSD with respect to the machined surface is variable, which obstructs locating the favorable angle range in practical detection. In addition, in order to locate the favorable angle range, it is inevitable to change the incident angle to the machined surface, which may enlarge the influence of the machined surface scattering, as stated in Section 3.1. In terms of the scattering under the s-polarized incident beam, the depolarization at the STC interface is slightly weaker than that under the p-polarized incident beam, but the depolarization at the CTS interface is more significant.

By further considering the distribution of SSD in the machined silicon, a decision can be made to use which polarization of the incident beam. Yin et al. [8] found that most cracks formed along and close to the {111} planes of monocrystalline silicon, resulting in most SSDs inclining to the ground surface at an angle of 40–60°. Based on the surface scattering characteristics, the vertical incidence to the machined surface is suggested for PLS detection, as mentioned in Section 3.1. In the vertical incidence to the machined surface, the incident angle of the SSD surface is equal to the inclined angle of SSD with respect to the machined surface, namely 40–60° for a machined monocrystalline silicon. In the incident angle range of 40–60°, it is obvious, as shown in Fig. 7, that the s-polarization incidence light leads to more depolarization of the scattering light than the p-polarization incidence light, i.e., the s-polarized laser incidence is more sensitive to detecting SSD than the p-polarized laser incidence in the PLS detection. Therefore, considering surface scattering, mechanical alignment of the detection system, and the depolarization of subsurface scattering, it is reasonable to use the s-polarized laser beam to vertically radiate the machined surface for the PLS detection of the machining-induced SSD in monocrystalline silicon.

Table 1
Grinding parameters for silicon wafers.

Parameters	Values
Grinding speed	44 m/s
Feed rate	90 μm/min
Wafer rotation speed	120 rpm
Grinding wheel	#320, #600

4. Experimental verification

4.1. Experimental setup

In order to verify the influence of surface scattering, a PLS detection system was constructed. The system used the vertically incident s-polarized laser to detect SSD, as shown in Fig. 8. The polarization s represents the polarization direction of the laser perpendicular to the incident plane, while the polarization p represents the polarization direction within the incident plane. A schematic diagram of the laser path is depicted in Fig. 8 (a) in which a laser beam is emitted from a laser, and travels through a polarizer, a polarized beam splitter (PBS), and is then reflected vertically to a lens to reach the silicon surface. Both the surface and subsurface scattering lights backscatter through the lens and get reflected by the reflector to reach PBS at which the backscattered lights are split. Finally, the depolarized light, i.e., p-polarization light, is received by a detector after filtered by a Glan polarizer, as indicated by the dashed arrows.

For the PLS detection system, it is important to detect SSD at different depths. The penetration depth of the incident beam should be large enough so as to detect SSD at all the depths. Generally, the depth of SSD induced in abrasive processes is in the order of tens of microns. The penetration depth is dependent on the laser wavelength. Zhang et al. [31] revealed that the laser penetration depth increased with the laser wavelength. In this study, the laser wavelength was 914 nm which could achieve about 200 μm penetration depth based on the optical transmission properties. Thereby, the refractive index of monocrystalline silicon $n = 3.61–0.002i$ at 914 nm. The experimental setup is shown in Fig. 8(b). A continuous-wave laser (MLL–III–914, CNI, China) with an emitted laser power of 15 mW was used as the laser source. The diameter of the laser beam was about 1.5 mm. The extinction ratios of the polarizer and PBS were 1:100 and 1:3 000, respectively. A Glan polarizer was used to ensure the received light is purely cross-polarized. The detector was a high-speed Si PIN photodiode (S3072, Hamamatsu, Japan)

Table 2
Experimental design of the PLS detection.

Sample No.	Surface roughness *Rq*/nm		SSD depth/μm	
	Low level(−)	High level(+)	Low level(−)	High level(+)
1		425	5.8	
2	275		5.3	
3		418		11.3
4	322		5.5	

with an amplification gain of 7.5 kV/W. The detected signal was recorded by a data acquisition device (PCIe6320, NI, USA). A translation stage was used to change the detection area of the silicon sample. The lens used to focus the incident laser beam was aspherical. The focal length of the lens was $f = 4.51$ mm. The numerical aperture of the lens was NA = 0.55. In this study the work distance between the lens and silicon wafer was 4.70 mm. The spot size of the incident laser beam on the silicon wafer surface was approximately 100 μm in diameter.

Before the experiments, stability and repeatability of the installed PLS detection system were tested. A completely polished wafer without SSD was used to test the stability of the system. A length of 10 mm was scanned by the PLS system to test the repeatability of the system. It was found that the overall variation of the detected PLS signal was within 5%. The wafers ground by the #320 and #600 wheels and polished wafers were used to calibrate the measurement. 10 different areas of each wafer were detected by the PLS detection system. It was found that the detected PLS signals of the wafers were distinctly different. The wafer ground by the #320 wheel represented the strongest PLS signal, followed by the wafer ground by the #600 wheel and polished wafer. The detected laser power of the wafer is about 20 μW for the wafer ground by the #320 wheel, 10 μW for the wafer ground by the #320 wheel, but only about 2 μW for the polished wafer. The coarser abrasive used in grinding, the larger damage induced into wafers. The detected PLS signal is dependent on the damage of the ground wafer. Therefore, the installed PLS detection system was suitable for the experimental verification.

In this study, the ground silicon wafers were used to verify the theoretical analysis of surface scattering and the application of the established PLS detection system. The silicon wafers were coarsely ground by the wafer self-rotation grinding so as to produce surfaces with larger surface roughness. Since a large surface roughness promotes the multi-scattering, it is beneficial to the verification of the influence of the surface roughness in the PLS detection. Grinding parameters are listed in Table 1. The Surface morphologies were characterized by a 3D interferometer (New View 5022, Zygo, USA). The surface height variation along the grinding marks is negligible compared to that in the direction

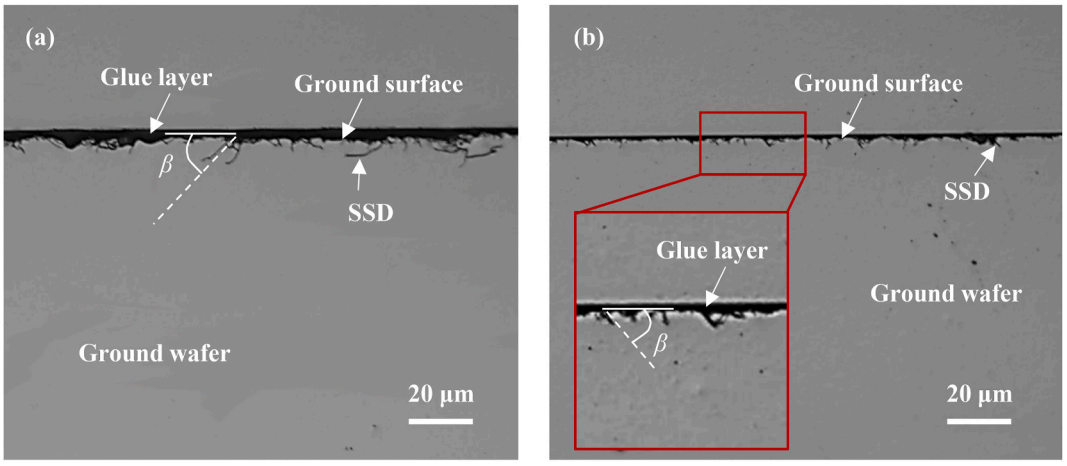

Fig. 9. Optical images of the cross-sectional view of the ground wafers. (a) The wafer ground by the #320 wheel; (b) the wafer ground by the #600 wheel.

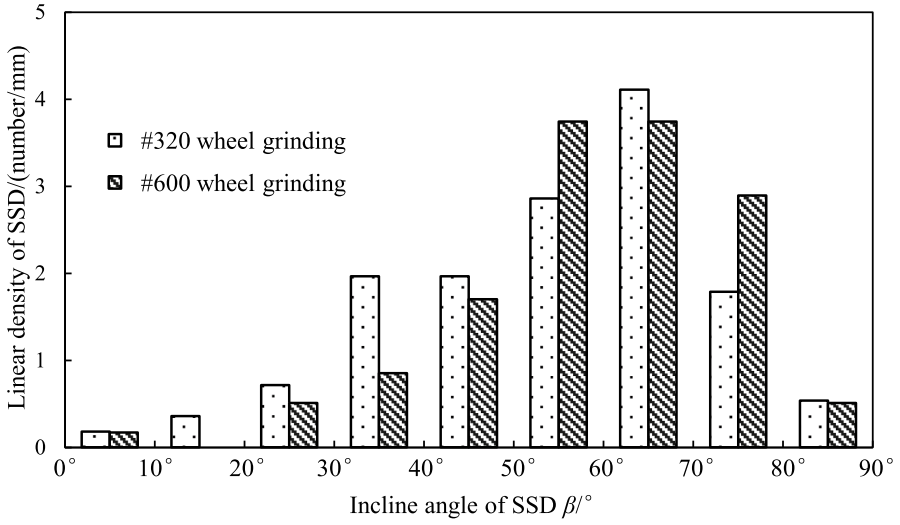

Fig. 10. Distributions of the incline angle of SSD in the ground wafers.

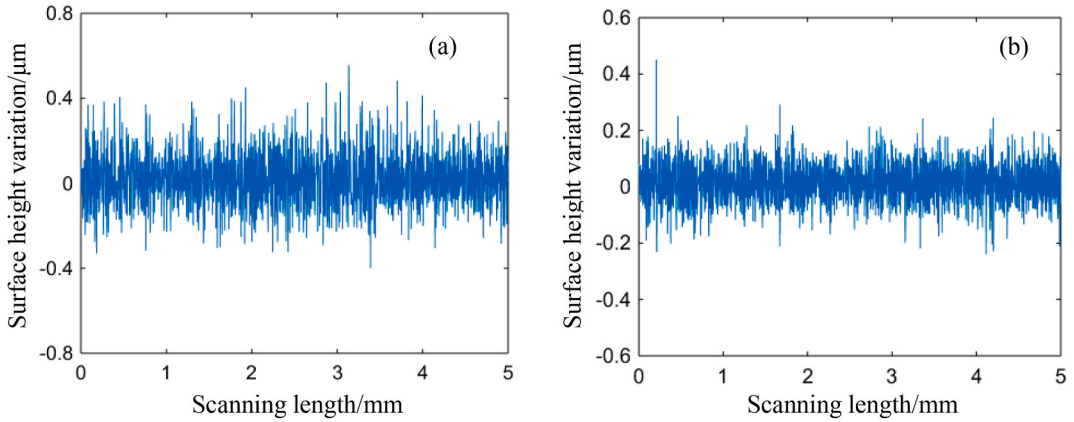

Fig. 11. Surface height variations of (a) the #320 wheel grinding surface and (b) the #600 wheel grinding surface.

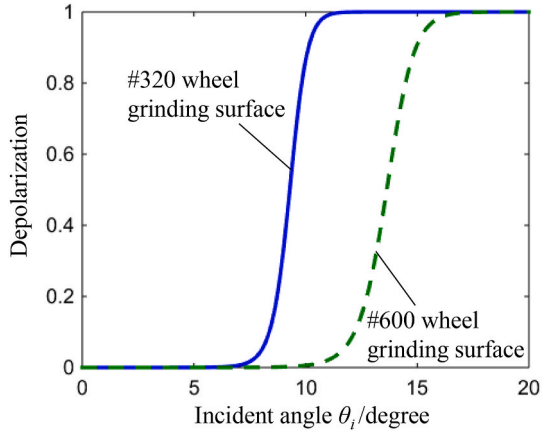

Fig. 12. Theoretical analysis of the depolarization caused by the ground surfaces at small incident angles, based on the experimentally determined surface roughness $Rq = 420$ and 375 nm and correlation length $S_{al} = 7.1$ and 5.0 μm for the #320 and #600 wheel grinding surfaces, respectively.

cross the grinding marks. Therefore, the ground surface profile could be regarded as one-dimensional variation. The surface profiles of the ground wafers were measured by a surface profilometer (Talysurf CLI2000, Taylor Hobson, USA) crossing the grinding marks. The depth of the grinding-induced SSD was obtained by the cross-sectional microscopy which was elaborated by Yin et al. [8]. The SSD depth of each sample was averaged over five measurements. Meanwhile, the inclined angles of SSD respect to the ground surface were measured. The number of the measured SSD in each wafer was near 100. The distribution of the incline angle of grinding-induced SSD was concluded so as to rationalize the design of the light path of the installed PLS system.

The silicon samples with different surface roughness and SSD depth were carefully selected and numbered for the PLS detection. The experimental design is shown in Table 2. Sample 1 and Sample 2 were at the same level of the depth of SSD but had different surface roughness (*Rq*), which is used to verify the influence of surface roughness. On the other hand, Sample 3 and Sample 4 possessing different SSDs were used to verify the SSD detection by the established PLS system. The PLS detection length was 5 mm with a step size of 0.5 mm. After detection, the influence of the surface roughness and SSD was revealed, which could verify detectability of the PLS system. During the PLS detection, the polarization direction of the incident laser was aligned with the grinding marks. According to a study by Yin et al. [18], the residual stress-induced photoelasticity was minimized in this study.

5. Results

The distributions of the grinding-induced SSD in the wafers are shown in Fig. 9. It can be seen that the #320 wheel grinding produced a larger depth of SSD than the #600 wheel grinding. SSD depth in the wafer ground by the #320 wheel was about 10 μm, as shown in Fig. 9 (a), whereas it was about 5 μm in the wafer ground by the #600 wheel, as shown in Fig. 9 (b).

The distributions of the incline angle of SSD are indicated in Fig. 10. Both the distributions of the incline angle represent a preponderant interval. Most SSD has an incline angle of 50–80° with respect to the

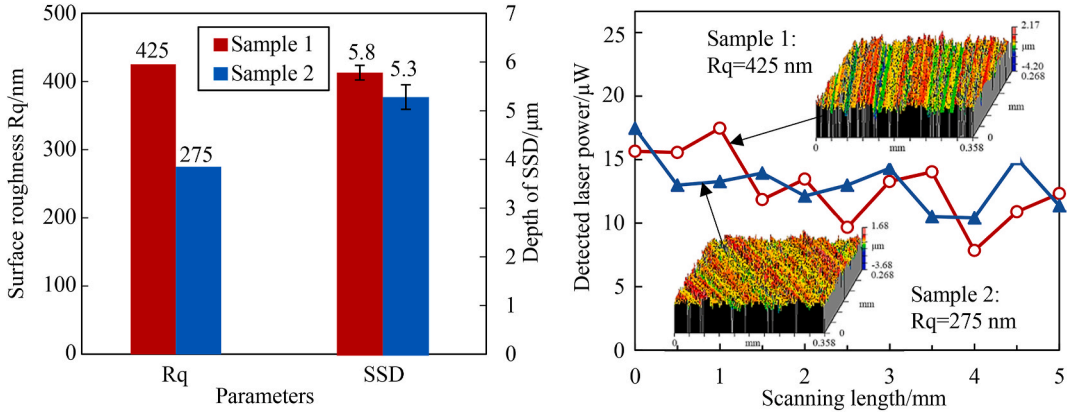

Fig. 13. Comparisons of Sample 1 and Sample 2: (a) the results of surface roughness Rq and SSD depth, (b) the distributions of the detected laser power in the PLS detection. The insets in (b) are the surface 3D morphologies of Sample 1 and Sample 2.

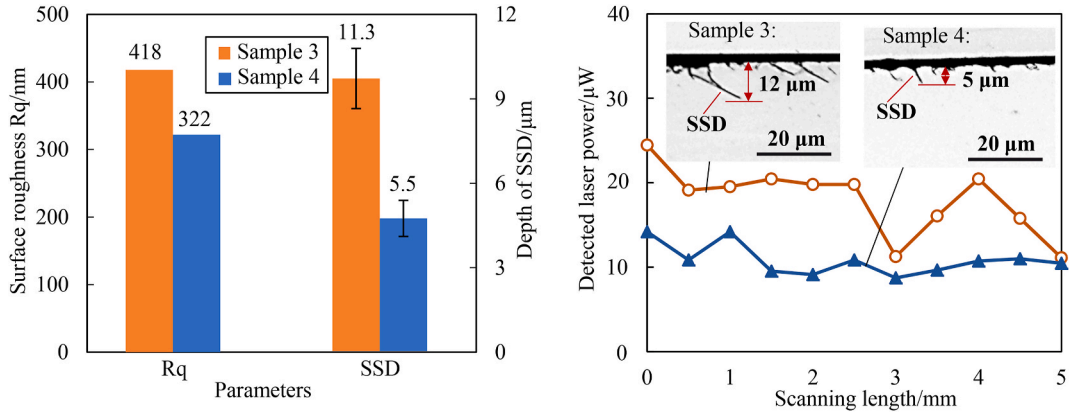

Fig. 14. Comparisons of Sample 3 and Sample 4: (a) the results of surface roughness Rq and SSD depth, (b) the distributions of the detected laser power in the PLS detection. The insets in (b) are the optical microscopic photos of SSD from Sample 3 and Sample 4.

ground surface, which is coincident with the previous study [8]. According to the theoretical results, shown as Fig. 7, it is partially rationalized that the PLS system is designed as vertical incidence to the wafers with the s-polarized laser.

The surface height variations along the direction crossing the grinding marks are shown in Fig. 11. It is noted that the variation amplitude of the surface ground by the #320 wheel is within ±0.4 μm, which is larger than that of the surface ground by the #600 wheel, that is within ±0.2 μm. The standard deviation σ (in fact the *Rq*-parameter value, obtained with filter settings λ_s = 2.5 μm and λ_c = 0.25 mm, Gaussian filter) and correlation length S_{al} of the ground surfaces were σ = 0.13 μm and S_{al} = 7.1 μm for the surface ground by the #320 wheel, whereas, σ = 0.10 μm and S_{al} = 5.0 μm for the surface ground by the #600 wheel. Based on Eqs. (13) and (14), the expected depolarization of surface scattering was calculated. The theoretical analysis of the depolarization caused by the ground surfaces is shown in Fig. 12. The depolarization could be neglected at the incident angle smaller than a critical value after which the depolarization increased dramatically. The critical value of the incident angle was about 8° for the #320 wheel grinding surface, smaller than about 12° for the #600 wheel grinding surface, which is mainly due to more multi-scattering caused by the larger surface roughness by the #320 wheel compared to the #600 wheel. Therefore, the vertical incidence of the PLS detection is effective for minimizing the surface scattering influence.

The surface roughness influence to the PLS detection is indicated in Fig. 13. As shown in Fig. 13 (a), Sample 1 and Sample 2 present similar SSD depth but obviously different surface roughness. However, the distributions of the detected laser power in the PLS detection can hardly be distinguished, as shown in Fig. 13 (b), which demonstrates that the surface roughness has little influence on the PLS detection.

A sample detection result of SSD is demonstrated in Fig. 14. As shown in Fig. 14 (a), Sample 3 presented almost the same surface roughness, but nearly doubled SSD depth of Sample 4. Correspondingly, the detected laser powers were distinctly different for the two samples. Sample 3 presented a larger SSD depth and detected laser power than Sample 4 in the PLS detection, as shown in Fig. 14. Therefore, the established PLS detection system is rationalized and can be used to detect the machining-induced SSD in monocrystalline silicon wafers.

Since the grinding marks are curves, the directions of the principal stresses is not constant in the region subjected to laser radiation. Although the photoelsticity is minimized in this study, it cannot eliminate the photoelasticity. The effect of photoelasticity is analyzed as follows. The power of the photoelasticity-induced depolarization light is determined by the angle θ between the polarization plane of the incident light and the first principal stress in the silicon wafer and the phase retardation ϕ, shown as Eq. (15) [5].

$$P = P_i \cdot D(\theta) \cdot D(\Delta\sigma) = P_i \cdot \sin^2(2\theta) \cdot \sin^2(\phi/2). \tag{15}$$

where P is the depolarized light intensity; P_i is the incident light intensity which is constant for a given laser power; $D(\theta) = \sin^2(2\theta)$ and $D(\Delta\sigma) = \sin^2(\phi/2)$ are defined as an angle-related coefficient and a stress-related coefficient, respectively. ϕ is the photoelasticity-induced phase retardation, given as Eq. (16).

$$\phi = \frac{2\pi C \cdot d}{\lambda}(\sigma_1 - \sigma_2). \tag{16}$$

where C is the stress-optic coefficient of silicon and varies in different orientations, λ is the wavelength of the incident light, d is the distance that light goes into the silicon wafer, σ_1 and σ_2 are the first and second principal stress, respectively. Based on the study by Yin et al. [5], C = 1.6×10^{-11} Pa^{-1}, d = 400 μm. According to the study by Zhou et al. [32], the difference between the first and second principal stresses may be up to several GPa. The stress-related coefficient $D(\Delta\sigma)$ varies within 0–1. The radiation spot size was 100 μm in diameter. The angle θ between the polarization plane of the incident light and the first principal stress should be less than 1° in such small region. Correspondingly, the angle-related coefficient $D(\theta)$ is less than 7.6×10^{-5}. Therefore, the power of the photoelasticity-induced depolarization light is less than 1.14 μW. According to Figs. 13 and 14, the detected laser power is generally over 10 μW. The variation caused by the photoelasticity is less 11.4%. Therefore, the effect of photoelasticty can be neglected in this study.

In a macro region, the directions of the principal stresses are aligned with the grinding marks. The effect of photoelasticty can be suppressed by the method proposed by Yin et al. [5]. Decreasing the radiation spot size can further decrease the effect of photoelasticty. Meanwhile, it can also increase the spatial resolution of the detection. However, when the radiation spot size decreases to several μm, the photoelasticity cannot be neglected. In such a micro region, the stress distribution is extremely uneven [33], it is complicated, the method for suppressing the effect of photoelasticty is inapplicable. The stress distribution in such micro region is still unclear, it needs further investigation. Therefore, the radiation spot size of the laser beam is here suggested to be far larger than several μm. According to the PLS detection, a larger depth of the damage provides a higher detected laser power for the ground wafers. By comparing with the results obtained by the traditional methods, the relationship between the detected PLS signal and the damage depth can be built. It can be used to evaluate the grinding-induced damage of the wafers.

The state of the polarization of the scattering light changes with the surface roughness, SSD, and polarization of the incident laser and the incident angle. Besides of the orthogonal component in this study,

ellipsometric and other polarizations can also occur [34], which makes the problem more complicated. Therefore, for the accurate measurement in the future, it is necessary to take into consideration of the Muller matrix which is applicable to determining all the polarization [35]. By then, the degree of the polarization has to be measured to reveal the polarization state of the scattering light.

6. Conclusions

This study presents a surface scattering model based on the EM scattering theory. According to the model, both surface and subsurface scatterings are elaborated. Then, based on the surface and subsurface scattering characteristics, a PLS detection system is designed and installed. The PLS detection system is used to detect SSD in a machined monocrystalline silicon. The feasibility of the installed PLS system is verified. The main conclusions are as follows.

(1) The surface scattering depolarization increases with surface roughness, surface correlation length, and incident angle. It is found that the surface influence to the PLS detection is minimized by adopting the vertical incidence.
(2) The design of the vertical incidence to the ground wafers with the p-polarized laser beam is demonstrated effective for detecting SSD by using the PLS method.
(3) The overall detected laser power of a ground wafer is mainly dependent on the SSD depth, rather than on the surface roughness. Therefore, the installed PLS detection system is applicable to detecting SSD in the machined monocrystalline silicon wafers.

Declaration of competing interest

The authors declare that they have no known competing financial interests or personal relationships that could have appeared to influence the work reported in this paper.

Acknowledgments

The study is supported by the Project Funded by China Postdoctoral Science Foundation (Grant Nos. 2020TQ0149 and 2021M691569) and National Natural Science Foundation of China (Grant Nos. 51575084 and 52105453).

References

[1] Sørensen B. 4 - the energy conversion processes. In: Sørensen B, editor. Renewable energy. fifth ed. Boston: Academic Press; 2017. p. 357–567. https://doi.org/10.1016/B978-0-12-804567-1.00004-9.
[2] Mukaida M, Yan J. Ductile machining of single-crystal silicon for microlens arrays by ultraprecision diamond turning using a slow tool servo. Int J Mach Tool Manufact 2017;115:2–14. https://doi.org/10.1016/j.ijmachtools.2016.11.004.
[3] Popa D, Ali SZ, Hopper R, Dai Y, Udrea F. Smart CMOS mid-infrared sensor array. Opt Lett 2019;44:4111–4. https://doi.org/10.1364/ol.44.004111.
[4] Zhang W, Allgood K, Biskach M, Chan K-W, Hlinka M, Kearney J, et al. Monocrystalline silicon and the meta-shell approach to building x-ray astronomical optics. SPIE; 2017.
[5] Yin J, Bai Q, Zhang B. Methods for detection of subsurface damage: a review. Chin J Mech Eng 2018;31:41. https://doi.org/10.1186/s10033-018-0229-2.
[6] Li HN, Yu TB, Zhu LD, Wang WS. Analytical modeling of grinding-induced subsurface damage in monocrystalline silicon. Mater Des 2017;130:250–62. https://doi.org/10.1016/j.matdes.2017.05.068.
[7] Zhang L, Chen P, An T, Dai Y, Qin F. Analytical prediction for depth of subsurface damage in silicon wafer due to self-rotating grinding process. Curr Appl Phys 2019;19:570–81. https://doi.org/10.1016/j.cap.2019.02.015.
[8] Yin J, Bai Q, Li Y, Zhang B. Formation of subsurface cracks in silicon wafers by grinding. Nanotechnology and Precision Engineering 2018;1:172–9. https://doi.org/10.1016/j.npe.2018.09.003.
[9] Wang L, Gao Y, Li X, Pu T, Yin Y. Analytical prediction of subsurface microcrack damage depth in diamond wire sawing silicon crystal. Mater Sci Semicond Process 2020;112:105015. https://doi.org/10.1016/j.mssp.2020.105015.
[10] Popovich VA, Verwaal W, Janssen M, Bennett IJ, Richardson IM. Application of X-ray computed tomography in silicon solar cells. In: 2010 35th IEEE photovoltaic specialists conference; 2010. https://doi.org/10.1109/PVSC.2010.5615872. 001759-001764.
[11] Brand S, Vogg G, Petzold M. Defect analysis using scanning acoustic microscopy for bonded microelectronic components with extended resolution and defect sensitivity. Microsyst Technol 2018;24:779–92. https://doi.org/10.1007/s00542-017-3521-7.
[12] Karabutov AA, Podymova NB. Study on the subsurface damage depth in machined silicon wafers by the laser-ultrasonic method. Case Studies in Nondestructive Testing and Evaluation 2014;1:7–12. https://doi.org/10.1016/j.csndt.2014.03.002.
[13] Shekhawat GS, Srivastava AK, Dravid VP, Balogun O. Thickness resonance acoustic microscopy for nanomechanical subsurface imaging. ACS Nano 2017;11:6139–45. https://doi.org/10.1021/acsnano.7b02170.
[14] Geiler HD, Karge H, Wagner M, Ehlert A, Daub E, Messmann K. Detection and analysis of crystal defects in silicon by scanning infrared depolarization and photoluminescence heterodyne techniques. Mater Sci Eng, B 2002;91–92:46–50. https://doi.org/10.1016/S0921-5107(01)00965-5.
[15] Geiler HD, Wagner M, Karge H, Paulsen M, Schmolke R. Photoelastic stress evaluation and defect monitoring in 300-mm-wafer manufacturing. Mater Sci Semicond Process 2002;5:445–55. https://doi.org/10.1016/S1369-8001(02)00138-5.
[16] Zhang JM, Sun JG, Pei ZJ. Application of laser scattering on detection of subsurface damage in silicon wafers. 2003. p. 15–24. https://doi.org/10.1115/IMECE2003-41105.
[17] Zhang JM, Sun JG. Quantitative assessment of subsurface damage depth in silicon wafers based on optical transmission properties. Int J Manuf Technol Manag 2005;7:540–52. https://doi.org/10.1504/IJMTM.2005.007702.
[18] Yin J, Bai Q, Zhang B. Subsurface damage detection on ground silicon wafers using polarized laser scattering. J Manuf Sci Eng 2019;141(10):101012. https://doi.org/10.1115/1.4044417.
[19] Yin J, Bai Q, Haitjema H, Zhang B. Two-dimensional detection of subsurface damage in silicon wafers with polarized laser scattering. J Mater Process Technol 2020;284:116746. https://doi.org/10.1016/j.jmatprotec.2020.116746.
[20] Zhang J. Laser scattering techniques for subsurface damage measurements: system development, experimental investigation, and theoretical analysis. Kansas State University; 2006.
[21] Hahn DW. Light scattering theory. Department of Mechanical and Aerospace Engineering, University of Florida; 2006.
[22] Li J, Zhang L, Qin Q-H. A regularized method of moments for three-dimensional time-harmonic electromagnetic scattering. Appl Math Lett 2021;112:106746. https://doi.org/10.1016/j.aml.2020.106746.
[23] Ozgun O, Kuzuoglu M. Implementation of coordinate transformations in periodic finite-element method for modeling rough surface scattering problems. Int J RF Microw Computer-Aided Eng 2016;26:322–9. https://doi.org/10.1002/mmce.20968.
[24] Jia C, Guo L, Li K. Graphics processor unit accelerated finite-difference time domain method for electromagnetic scattering from one-dimensional large scale rough soil surface at low grazing incidence. J Appl Remote Sens 2014;8:1–10. https://doi.org/10.1117/1.JRS.8.084795.
[25] Fuks IM. Backscattering from a statistically rough 2-D surface: diffraction corrections to geometrical optics cross sections. Radio Sci 2007;42. https://doi.org/10.1029/2007RS003637.
[26] Yang P, Guo L. Polarimetric scattering from two-dimensional dielectric rough sea surface with a ship-induced kelvin wake. Int J Antenn Propag 2016;2016:2474708. https://doi.org/10.1155/2016/2474708.
[27] Fung AK, Li Z, Chen KS. Backscattering from a randomly rough dielectric surface. IEEE Trans Geosci Rem Sens 1992;30:356–69. https://doi.org/10.1109/36.134085.
[28] Li Z, Fung AK. A reformulation of the surface field integral equation. J Electromagn Waves Appl 1991;5:195–203. https://doi.org/10.1163/156939391X00563.
[29] Haitjema H. Reflectivity. In: Laperrière L, Reinhart G, editors. CIRP encyclopedia of production engineering. Berlin, Heidelberg: Springer Berlin Heidelberg; 2014. p. 1042–4. https://doi.org/10.1007/978-3-642-20617-7_15.
[30] Pei ZJ, Billingsley SR, Miura S. Grinding induced subsurface cracks in silicon wafers. Int J Mach Tool Manufact 1999;39:1103–16. https://doi.org/10.1016/S0890-6955(98)00079-0.
[31] Zhang JM, Sun JG, Pei ZJ. Optical transmission properties of silicon wafters: theoretical analysis. In: ASME 2004 international mechanical engineering congress and exposition; 2004. p. 17–24. https://doi.org/10.1115/imece2004-59195.
[32] Zhou P, Yan Y, Huang N, Wang Z, Kang R, Guo D. Residual stress distribution in silicon wafers machined by rotational grinding. J Manuf Sci Eng 2017;139:81012–7. https://doi.org/10.1115/1.4036125.
[33] Chen P, Zhang ZW, An T, Yu HP, Qin F. Generation and distribution of residual stress during nano-grinding of monocrystalline silicon. Jpn J Appl Phys 2018;57(12):121302. https://doi.org/10.7567/jjap.57.121302.
[34] Azzam RMA, Bashara NM. Ellipsometry and polarized light. 2003. North-Holland.
[35] Márquez A, Moreno I, Iemmi C, Lizana A, Campos J, Yzuel MJ. Mueller-Stokes characterization and optimization of a liquid crystal on silicon display showing depolarization. https://doi.org/10.1364/OE.16.001669; 2008. 16(3):1669-1685.